Journal of Marine Systems 204 (2020) 103285

Contents lists available at ScienceDirect

Journal of Marine Systems

journal homepage: www.elsevier.com/locate/jmarsys

An assessment of the East Australian Current as a renewable energy resource

Amandine Schaeffer[a,b,*], Matthew R. Archer[a], Quentin Baumard[a], Moninya Roughan[a,b], Colette Kerry[a]

[a] School of Mathematics and Statistics, UNSW Sydney, NSW 2052, Australia
[b] Center for Marine Science and Innovation, UNSW Sydney, NSW 2052, Australia

ARTICLE INFO

Keywords:
Marine kinetic energy
Western boundary current
Ocean renewable energy
Ocean currents
Hydrokinetic energy flux
Power density

ABSTRACT

Ocean currents are an energy resource that could be harnessed to increase renewable energy yields and reduce humanity's dependence on fossil fuels. The first challenge is to identify regions of significant kinetic energy flux that are a viable distance from the shore for the extraction and transport of energy. Western boundary currents (WBCs) have been identified as the most promising resource in this regard due to their strong current speeds (typically 1–2 m s^{-1}). However, such a resource is by necessity regional, so each prospective region requires thorough investigation. While global studies of WBCs (including the East Australian Current, hereafter the EAC) have been conducted using numerical models, they have coarse resolutions and often underestimate kinetic energy, which is the specific resource that needs accurate assessment. Here we address this knowledge gap, using a range of current velocity observations from moorings, high frequency radar and satellite altimetry to investigate the potential of the EAC as a future renewable energy resource, at various latitudes along the east Australian coast. Finally, in combination with a high-resolution data assimilating model, we propose the optimal location for future energy extraction opportunities with relatively high hydrokinetic flux (average of ~ 500 W m^{-2} at 50 m depth), constant direction and suitable location (25 km from shore in 400 m seawater depth).

1. Introduction

In the context of a changing climate, the need to reduce carbon emissions in combination with ever-increasing energy demands makes the transition from fossil to renewable clean energy critical. While solar and wind energy are now commercially used, Ocean Renewable Energy (ORE) is attracting growing interest. This includes potential energy, like ocean thermal energy conversion (OTEC) and tidal barrage, and kinetic energy from waves and tidal currents in channels (Chen et al., 2018; Dhanak et al., 2016). Moreover, recent studies have identified marine kinetic energy (MKE) from non-tidal oceanic currents as a prospective source of energy supply (e.g. Hammar et al., 2012; Hanson et al., 2016). Compared with tidal energy, such large-scale currents have the advantage of flowing in one major direction with less temporal variability, but are less predictable and in greater water depth. The technology is still in development, but it will likely consist of a moored sub-marine turbine with a horizontal axis, similar to that used for wind and tidal turbine designs (Neary et al., 2014). Although ocean currents are significantly slower than winds, the density of seawater (800 times larger than air) compensates for the slower speed, resulting in ocean currents with a similar capability for energy generation (Bane et al., 2017). In particular, Western Boundary Currents (WBCs), which are highly energetic currents in the global ocean that typically flow adjacent to highly populated regions (e.g. east coasts of the USA, Japan and Australia), are good candidates for harvesting MKE (Bane et al., 2017).

While the extraction of MKE from WBCs is still in an early stage of development, there is a growing interest globally (Council, 2013). Most studies have focused on the Gulf Stream along the US, (Bane et al., 2017; Dhanak et al., 2016; Hanson et al., 2010; Lowcher et al., 2017; Yang et al., 2013, 2015), the Kuroshio along Japan, (Chang et al., 2015; Chen, 2010) and Agulhas current along South Africa (Meyer et al., 2017) as the most energetic WBCs globally that can provide in excess of 1000 W m^{-2} in power density. Global studies by VanZwieten et al. (2014) and Dhanak et al. (2016) also identify WBCs along Australia, Somalia, Madagascar, and Brazil as areas profitable for power extraction (in excess of 500 W m^{-2}). To date, only two studies have investigated MKE specifically in Australian waters (Griffin and Hemer, 2010; O'Callaghan and Chabchouc, 2018), and they are based on coarse-resolution models that tend to underestimate the current speed and hence the power available. Therefore, local higher-resolution

* Corresponding author at: School of Mathematics and Statistics, UNSW Sydney, NSW 2052, Australia.
E-mail address: a.schaeffer@unsw.edu.au (A. Schaeffer).

https://doi.org/10.1016/j.jmarsys.2019.103285
Received 17 January 2019; Received in revised form 26 November 2019; Accepted 17 December 2019
Available online 23 December 2019
0924-7963/

studies are necessary to accurately determine the available resource for Australia.

The East Australian Current (EAC) is the WBC of the South Pacific sub-tropical gyre that flows along the narrow continental shelf in the Tasman Sea off eastern Australia. Although it is the weakest of the five major WBCs (VanZwieten et al., 2014), it is conveniently located off the most populated and energy-consuming coast of the country, which facilitates transportation of future extracted energy and connection to the grid. Griffin and Hemer (2010) first discussed the EAC as a potential energy resource as part of a broader study that focused on wave ORE; based on their 0.1°-resolution ocean model they calculated a median speed at each grid cell reaching 0.9 m s^{-1} (equivalent to a power density $P_d \approx 374 W\ m^{-2}$), concluding that such assessment requires in situ validation. O'Callaghan and Chabchouc (2018) used a 1/8th degree data-assimilating ocean state estimate (ECCO 2) to study the ocean current magnitude in the region, but focused on downstream mesoscale eddies and their propagation rather than the more stable current jet at lower latitudes along the coast. To date, only temporal averages of the EAC power densities are available in global studies, varying significantly based on the modelling study ($P_d = 583\ W\ m^{-2}$ in VanZwieten et al. (2013) and $P_d = 730\ W\ m^{-2}$ in Dhanak et al. (2016) at 50 m depth).

To address the lack of a systematic resource assessment for the EAC, in this study we use a suite of high-resolution in situ and remote observations to assess its power density, and try to inform best implementation for future pilot engineering studies based on a data-assimilating high resolution ocean model. This study is a critical first step in the extraction of hydrokinetic energy from the EAC. We focus on quantifying the potential capacity of this resource, irrespective of present engineering constraints which will improve with developing technologies by the time such energy extraction becomes commercially viable. This assessment provides the fundamental information needed to inform future project development of ocean extraction devices in Australia's WBC.

2. Dataset and methods

2.1. Observation platforms

Ocean observations around Australia's coastline are made available by Australia's Integrated Marine Observing System (IMOS, http://www.imos.org.au). Data can be accessed via the Australian Ocean Data Network (AODN) portal (http://www.aodn.org.au).

2.1.1. Satellite altimetry

Daily satellite surface geostrophic velocities between 2012 and 2018 were sourced from IMOS remote sensing branch (Deng et al., 2010). The gridded dataset was created using optimal interpolation of altimeter and tidegauge data to estimate the sea surface height (SSH), resulting in an improved estimate of geostrophic velocities, particularly across the continental shelf. The final product has a daily resolution of 1/5° and gives a synoptic view of the SSH and the mesoscale ocean currents, but does not resolve the shelf dynamics nor the high temporal variability. Indeed Schaeffer et al. (2016) showed great disparities between satellite and in situ current velocities on the shelf in this area.

2.1.2. High frequency radar

High-resolution ocean surface current measurements are made by two WERA phased-array HF radar systems, deployed along the east Australian coast at Red Rock (30.0°S) and North Nambucca (30.6°S) (Fig. 1). The two systems transmit at a frequency of 13.92 MHz, observing the radial component of velocity (towards/away from radar) averaged over the top 0.9 m of water depth, at a spatial resolution of 1.5 km out to approximately 150 km. The exact range varies in time, being dependent on sea state and ambient radio interference (Gurgel et al., 1999).

Here we utilize raw radial velocities (Cosoli et al., 2018) between 5 Mar 2012 to 22 Dec 2016 sub-sampled to three hours. Quality control procedures for both the radial and vector data used here are described in Archer et al. (2017). To account for regions of large geometric dilution of precision (GDOP, Chapman et al., 1997) values and high noise, we remove grid points that comprise intersecting angles exceeding 135° or less than 45°, and latitudes < 30°S or > 30.6°S. This dataset has been evaluated by Wyatt et al. (2018), who concluded it can be used with confidence for scientific analysis.

To investigate variability of the EAC in speed and location, we first identify its core at latitude 30.27°S, which we define as the maximum poleward surface speed of the jet at each snapshot in time, following the method of Archer et al. (2017). This also provides a time series of the EAC jet core movement (meandering), in units of longitude.

2.1.3. Shelf mooring

A shelf mooring was deployed in 2010, 25 km off Coffs Harbour at 30°S in 100 m of water (hereafter CH100; at 153.40°E, 30.27°S, Fig. 1), and is still operating to-date. We use current velocity observations between 2010–2018 from the bottom-mounted acoustic Doppler current profiler (ADCP; see Schaeffer et al. (2013) for more details). Measurements have a temporal and vertical resolution of 5 min and 8 m bins, daily averaged, with bad data removed in the surface and bottom 10–15 m.

2.1.4. Deep-water mooring

A full-depth (surface to 4000 m) deep-water mooring array extends offshore Brisbane, at 27°S, and is comprised of five deep water moorings (labelled EAC 1–5). The mooring array was positioned where the EAC is predicted to be most coherent and designed to measure the mean and time-varying EAC transport. Each mooring has a suite of instruments measuring temperature, salinity, and velocities at high sampling frequencies (5 min, 5 min, and 30–60 min, respectively) throughout the water column. Here we use ADCP current measurements from the upward looking ADCP (nominal depth of 81 m) at EAC2 site (also called EAC_ M2, bottom depth of 1940 m, at 153.99°E, 27.3°S) between 20-Apr-2012 and 28-Aug-2013, which is the closest site from the EAC core (Sloyan et al., 2016). Details of the instruments and sampling can be found in Sloyan et al. (2016).

2.2. Data-assimilating model

In order to assess the power density across the region and at locations not directly sampled by observations, we make use of outputs from a high-resolution data-assimilating model of the EAC region (Kerry et al., 2016). The model combines a state-of-the-art numerical ocean model with a variety of traditional and newly available observations with 4-dimensional variational data assimilation (4D-Var) to generate a dynamically-consistent 'best-estimate' of the ocean state over a 2-year period (2012–2013). The numerical model is configured using the Regional Ocean Modelling System (ROMS, Moore et al., 2011) with a 2.5–6 km horizontal resolution and 30 vertical sigma-layers distributed with a higher resolution in the upper 500 m. Assimilated observations include surface radial velocity observations from the HF radar array, and velocity and hydrographic measurements from continental shelf moorings and the deep-water mooring array (all described in Section 2.1). Hydrographic measurements from autonomous ocean gliders, as well as from more traditional data streams (satellite-derived sea surface height, SSH, and sea surface temperature, SST, temperature and salinity from Argo profiling floats and temperature profiles from Expendable Bathythermograph, XBT, lines) are also assimilated.

The two year reanalysis has been rigorously evaluated against a range of assimilated and independent (non-assimilated) observations by Kerry et al. (2016). They show that the root mean square differences between the observations and the analysis (the analysis error) is significantly lower than the error in the non-assimilating free running

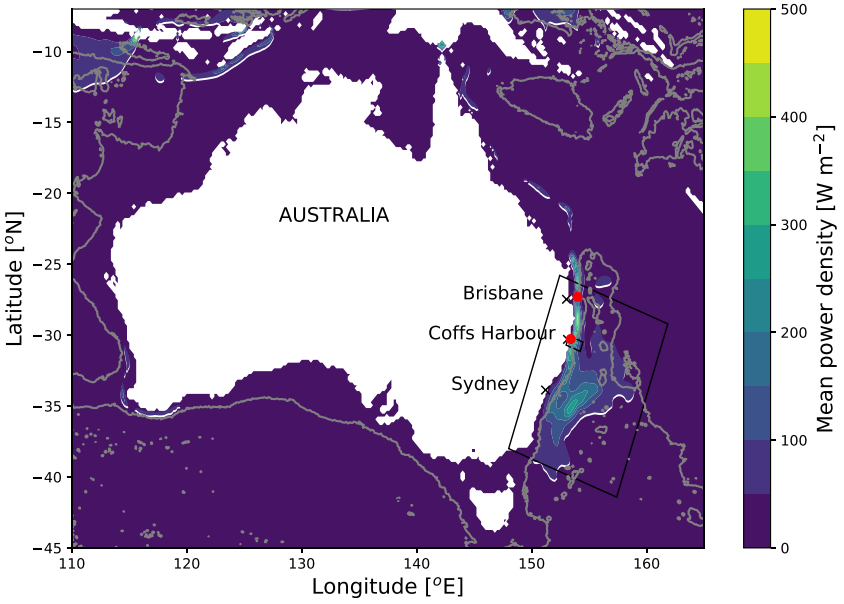

Fig. 1. Mean power density over 2012–2018 calculated from daily satellite geostrophic velocities. The 2000 m isobath is overlaid in grey. The location of moorings EAC2 (off Brisbane) and CH100 (off Coffs Harbour) are shown by red circles, and the main east coast cities by black crosses. Boxes show the HF radar coverage off Coffs Harbour (smaller box) and the model domain (larger box). (For interpretation of the references to color in this figure legend, the reader is referred to the web version of this article.)

model. This is true for both surface observations e.g. SSH, SST, and surface currents from the HF radar system (Kerry et al., 2016, their Figs. 2, 9, 10, 14) and subsurface observations from Argo floats, moorings and independent Conductivity-Temperature-Depth (CTD) casts (Kerry et al., 2016, their Figs. 12, 13, 15).

The model output has been used successfully in a number of studies e.g. for understanding observation impact in the EAC System (Kerry et al., 2018). Thus we are confident that this model provides a reliable ocean-state estimate for the EAC System. Moreover it is the most suitable model available for the analysis presented here, due to its high resolution, refined bathymetry, and data assimilation. Full details of the model configuration and performance can be found at Kerry et al. (2016, 2018).

2.3. Hydrokinetic power density and environmental parameters

The kinetic energy flux, or power density (P_d) per unit area perpendicular to the flow, is used to estimate the MKE available, which is the key variable to consider when choosing a location for electricity generation based upon the resource. The power density is estimated as $P_d = \frac{1}{2}\rho S^3$ [W m^{-2}], with ρ the density taken as 1025 kg m^{-3} (in agreement with local glider observations, Schaeffer et al., 2016) and the current Speed $S = \sqrt{(u^2 + v^2)}$ [m s^{-1}], calculated from u and v, the eastward and northward components of the current velocity, respectively (e.g. Bane et al., 2017). MKE is extracted from ocean currents using large turbines that require energy to get them moving initially. A cut-in speed (S_{start} or start-up speed) is usually considered, below which the amount of energy required to operate the turbines is greater than the amount of energy produced. Depending on the device engineering, S_{start} is set to 0.5 m s^{-1} or 1 m s^{-1} (even 1.5 m s^{-1} in Hanson et al., 2010), equivalent to $P_d \sim 64$ W m^{-2} or $P_d \sim 512$W m^{-2}) (Bane et al., 2017; Meyer et al., 2017; VanZwieten et al., 2014).

Various other factors should be taken into account in the context of energy extraction (Chang et al., 2015). Due to the expected large diameters of the turbines and surface disturbance (boat traffic, waves, weather etc.) estimates of the sub-surface flow is necessary. We choose a depth of 50 m (Dhanak et al., 2016), while other studies typically focuses on depths around 25 and 75 m (Bane et al., 2017; Tseng et al., 2017). In addition, the deeper and further from the coast, the more challenging and expensive the engineering, installation and maintenance aspects will be. This is due to difficulties for anchorage at great depths, high pressure on the system, and integration to the grid through power transmission cables. Hence the distance from the coast and local water depth are important parameters to consider when investigating potential sites. We also investigate the temporal variability of the kinetic fluxes since fluctuating electric power is still an important consideration for a connection to the grid, despite technological progress in energy storage (Esteban and Leary, 2012).

3. Regional view

The EAC is Australia's strongest current, flowing poleward along the east coast of Australia from where it forms at ~22°S to where it separates from the coast most often at ~ 31–32.5°S (Cetina-Heredia et al., 2014) (Fig. 1). The EAC is most coherent at 28°S (Sloyan et al., 2016), however, it strengthens along its path to a maximum velocity on the continental shelf at around 30–32° S (Schaeffer and Roughan, 2015), where it can reach maximum speeds up to 2.5 m s^{-1} (Archer et al., 2017), and depth-averaged velocities of 0.5 m s^{-1} on the shelf (Schaeffer et al., 2013). At the separation point, energetic anticyclonic mesoscale eddies are shed from the jet towards the east and south, while broadening and deepening (Kerry et al., 2018; Oke et al., 2019). The mean power density calculated from daily satellite geostrophic velocities between 2012 and 2018 shows a maximum of 440 W m^{-2} around 29°S. While this is less than other WBCs (VanZwieten et al., 2014), this is likely underestimated due to the coarse resolution of the geostrophic velocity dataset that does not resolve the smaller-scale geostrophic and ageostrophic current velocities.

Indeed, the maximum mean power density at the surface computed from radar-derived ocean current observations is P_d = 839 W m^{-2} at 30.6°S, which is significantly larger than that derived from the coarse geostrophic velocities. The location of maximum P_d matches the mean location of the EAC core above the 1500–2000 m isobath at a distance of about 40–50 km from land at this latitude (Fig. 2a).

4. Temporal variability

Fig. 2d shows the lateral movement of the EAC as a time-series of the jet core longitude. At latitude 30.27°S, the jet meanders in longitude with a range that can exceed 80 km at the most extreme, but with a standard deviation of 20 km. The power density averaged following the core of the EAC is 1521 W m^{-2} (Fig. 2c), but with a large temporal variability (a maximum of 10,000 W m^{-2}) and values exceeding 500 W m^{-2} 82% of the time that data is recorded. While such a jet-

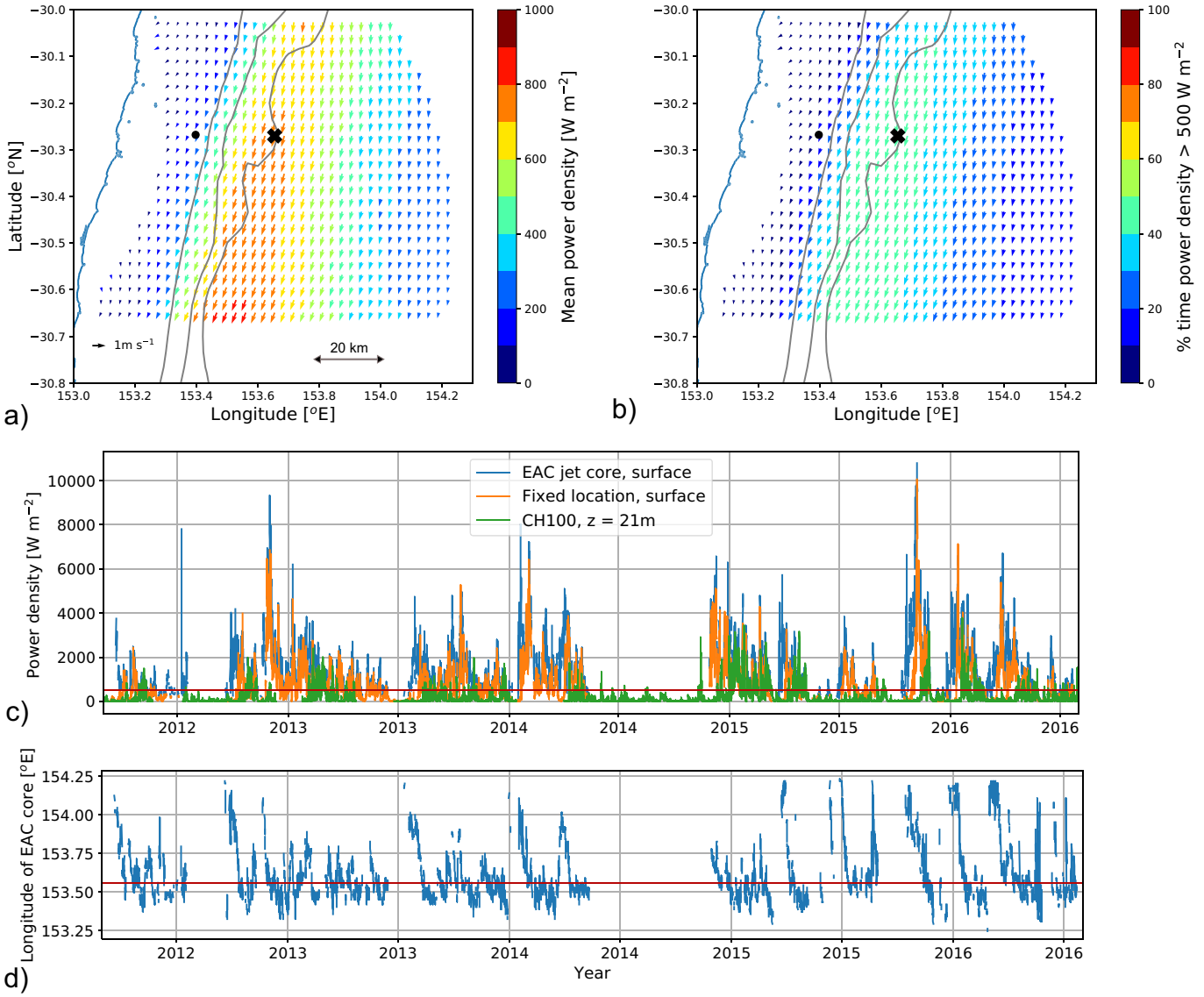

Fig. 2. (a) Surface mean power density and (b) percentage of time $P_d > 500$ W m^{-2} calculated from HF radar current velocities; The 200-, 1000- and 2000-m isobaths are shown in grey. (c) Time-series of power density in the EAC jet core (latitude −30.27) and at a fixed location (153.65, −30.27) from surface HF radar measurements, and at CH100 mooring from ADCP measurements at 21 m depth (153.40, −30.27). (d) Time-series of the EAC jet core longitude at latitude −30.27. In the maps, the fixed-location position is denoted by a black cross, and mooring CH100 denoted by a black circle. The red horizontal line shows the threshold of 500Wm^{-2} in (c) and the median core longitude in (d). (For interpretation of the references to color in this figure legend, the reader is referred to the web version of this article.)

following average clearly highlights the maximum potential of the jet, a turbine would typically be in a fixed location, hence a calculation at a fixed point is more meaningful for energy extraction. Choosing the location with the maximal mean P_d at the same latitude (153.65°E, 30.27°S, location shown in Fig. 2a, b), P_d is reduced to a temporal average of 730 W m^{-2}, and exceeds 500 W m^{-2} only 45% of the time (Fig. 2b). This reduction in mean power is a result of the meandering motion of the jet core, so that at times the flow is weak in the vicinity of any fixed-location.

The 5-year timeseries of power density qualitatively reveals its variable character across a range of time scales. As previously shown (Archer et al., 2017), the EAC speed, and hence its power density, exhibit a clear annual cycle (Fig. 3). Austral summer monthly means largely exceed 500 W m^{-2} both for the EAC jet core and the fixed-location (Fig. 3a). However, while the minimum monthly means in the jet core are still greater than the threshold (636 W m^{-2} in June), the minimum power density at the fixed-location is 155 W m^{-2} in June, which is well below the minimum threshold of 500 W m^{-2} suggested by VanZwieten et al. (2014). The power density also exhibits inter-annual variability, although the amplitude is less than the annual cycle over the 5 years of data available (Fig. 3b). Note that the anomaly in 2014 can partially be attributed to missing data in winter months leading to a mean that is biased towards summer months when the EAC is faster.

A frequency power spectrum of P_d in the EAC core (Fig. 4) confirms the annual cycle and also reveals highest variability occurs at periods between 60 and 70 days. This is the so-called ‘ eddy-shedding time-scale’, associated with mesoscale anticyclonic eddy-shedding events at the EAC separation zone (Mata et al., 2006; Oke et al., 2019 for an in-depth review). Shorter-period fluctuations of P_d at 20 days have been noted previously by Archer et al. (2017) in core speed, associated with the meandering of the EAC (their Fig. 7). The fixed location P_d exhibits the same periodicity as the jet core, but with lower energy, and some smearing of spectral variance due to the meandering of the jet over the

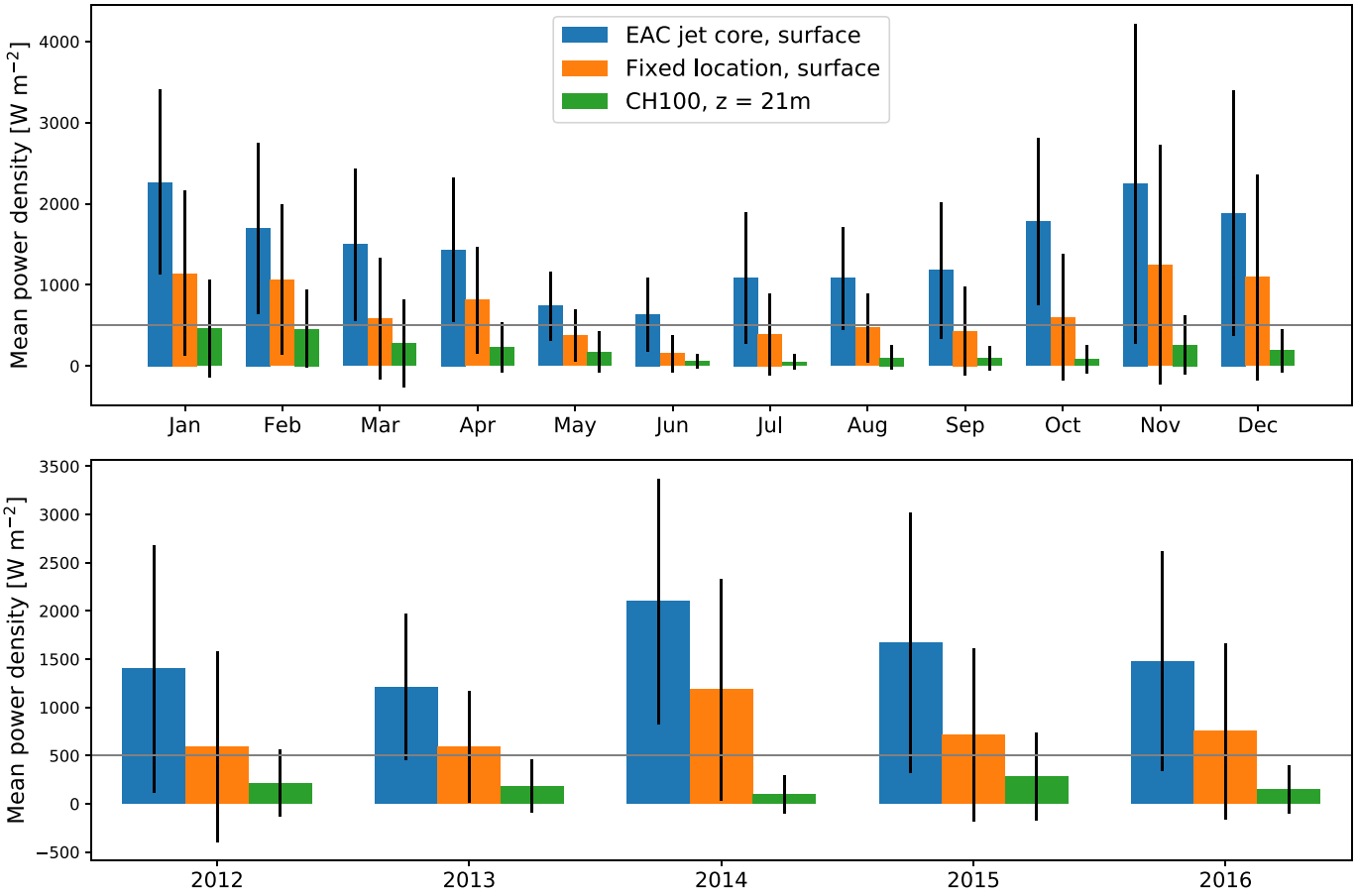

Fig. 3. Monthly (top) and annual (bottom) means (bars) and standard deviations (black lines) of power density at the EAC jet core and a fixed location from surface HF radar measurements, and at CH100 mooring from ADCP measurements at 21 m depth (positions shown in Fig. 2). Grey horizontal line shows the threshold of 500 W m^{-2}.

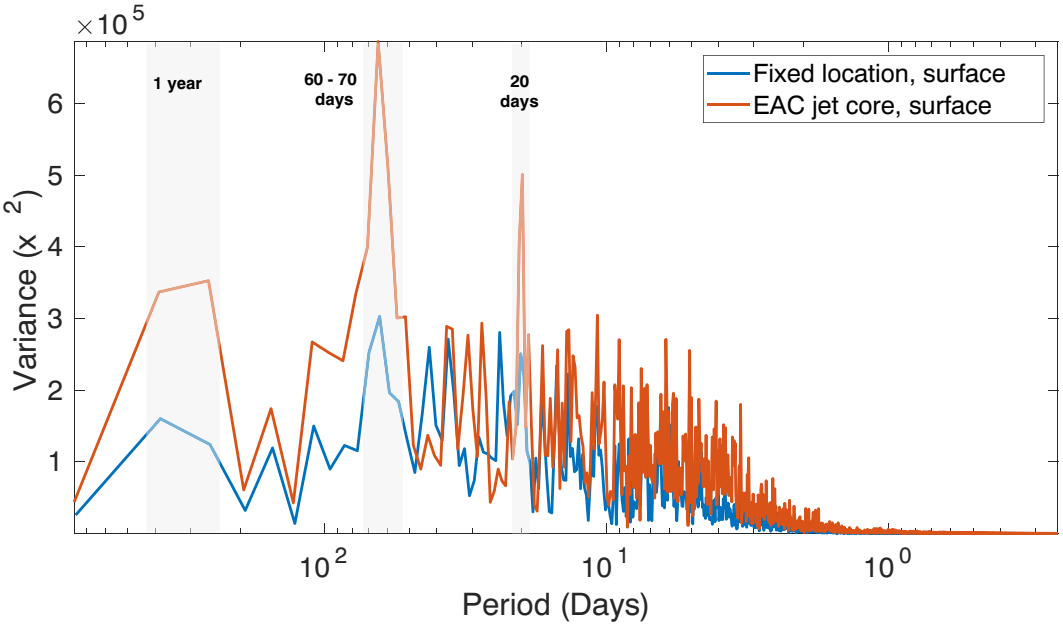

Fig. 4. Variance-preserving frequency power spectra of surface P_d from HF radars time-series at (blue) a fixed-location, and (red) following the EAC jet core. Dominant peaks of variability are highlighted by the shaded columns at: 1 year, 60–70 days, and 20 days. The spectra are computed using Welch's averaged periodogram method, with X the units (m s^{-}1) half-overlapping segments Hanning windowed in the time domain, Fourier transformed, and ensemble averaged. (For interpretation of the references to color in this figure legend, the reader is referred to the web version of this article.)

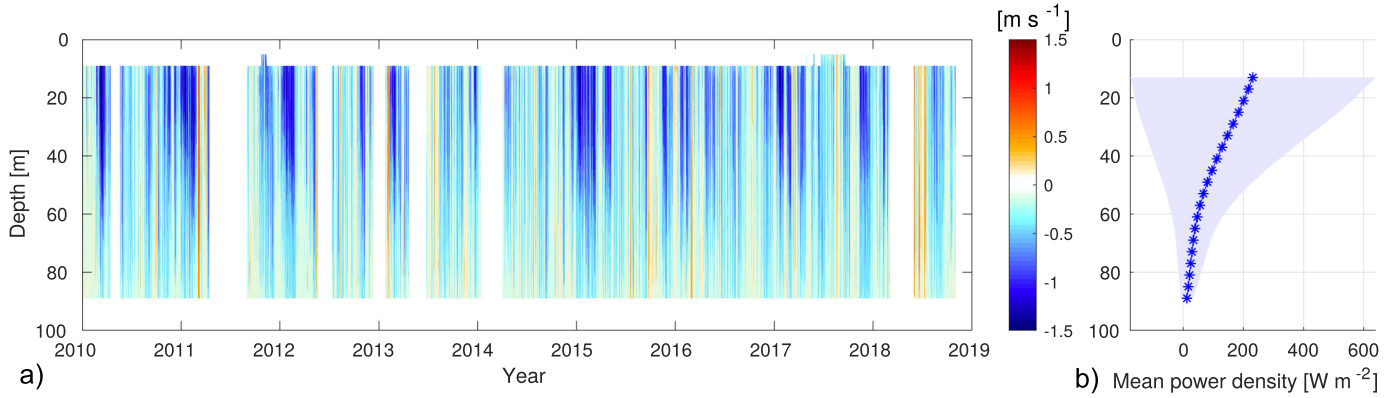

Fig. 5. Temporal evolution over depth of alongshore current velocity (a) and mean power density with shaded standard deviation (b) calculated at CH100 mooring (location shown in Fig. 2).

geographic location.

5. Depth variability

Despite a recent study suggesting a sub-surface maximum of the EAC further offshore (Sloyan et al., 2016), long term velocity observations on the shelf show a decreasing mean speed with depth (Fig. 5), in agreement with other WBCs (Dhanak et al., 2016; Imawaki et al., 2013; VanZwieten et al., 2013). At mid-shelf (25 km offshore at 30.27°S), in water depth of 100 m, the circulation is dominated by the western edge of the EAC rather than its core (see Fig. 3a), leading to average southward velocities measured at CH100 mooring around 0.44 m s^{-1} (P_d = 217 W m^{-2}) at 17 m depth, decreasing to 0.3 m s^{-1} (P_d = 80 W m^{-2}) at 50 m and 0.10 m s^{-1} (P_d = 12 W m^{-2}) at 90 m depth (Fig. 5). The time-series show high variability in intensity (Figs. 5 and 3c), but a consistent southward direction at all depths most of time (negative along-shelf velocity), with limited counter-current episodes in response to southerly winds or eddies (Schaeffer et al., 2013; Wood et al., 2016). These observations confirm that the flow is mostly barotropic on the shelf, and weakening with depth. However, as the current is strongest over the ~ 1500 m isobath at this latitude, sites further offshore would allow greater energy extraction.

Another useful data source is the full-depth mooring array described by Sloyan et al. (2016) off Brisbane (~ 27°S), extending the full depth of the water column to greater than 4000 m. ADCPs are attached to the mooring lines, as opposed to the bottom-mounted ADCP used in Fig. 5. These observations reveal recurrent high power density reaching > 900 W m^{-2} (Fig. 6) but missing values prevent us from computing temporal averages in shallow depths. Strong currents induce a tilting of the mooring line, leading to important variations of the instrument actual depth. In the particular example at the mooring in 2000 m water depth (Fig. 6), the ADCP is upward looking and oscillates between depths between of 80 m and 250 m, as indicated by the pressure measured by the instrument. Hence measurements of the current velocity in the top layers (< 80 m depth) only occur during episodes of weak current when the mooring line is not tilted. This example illustrates technical issues with deep sea moorings that are likely to translate to floating turbine technology with long anchor chain length in regions of strong currents. Similar difficulties in mooring performance have been experienced in other WBCs, e.g. Archer et al. (2015) measured large pitch and roll values from an ADCP attached to a mooring line being pushed down in the Florida Current, caused by the strong drag on the mooring line by the fast-flowing current.

6. Optimal sites for energy extraction

As observational datasets are limited in spatial coverage, especially at depth, the data-assimilating ROMS model allows us to investigate power density distribution over a range of latitudes and depths where observations are not available. Considering the potential technical issues arising from deep anchorage discussed in the previous section, we focus on the current above the 400 m isobath. Along the coast, one can see the variable influence of the EAC on the shelf (Fig. 7), with latitudes where it is mostly flowing further offshore leading to weak transport above the 400 m isobath (e.g. ~ 30.5°S and 27°S, Fig. 7d), and latitudes where it flows close to the coast and the mean power density above the 400 m isobath is elevated.

The region of maximum mean power density at 50 m depth is between 31.3°S and 32.2°S, where it is greater than 500W m^{-2}. This is where the shelf is narrow and the EAC jet accelerates (Fig. 7a). This is

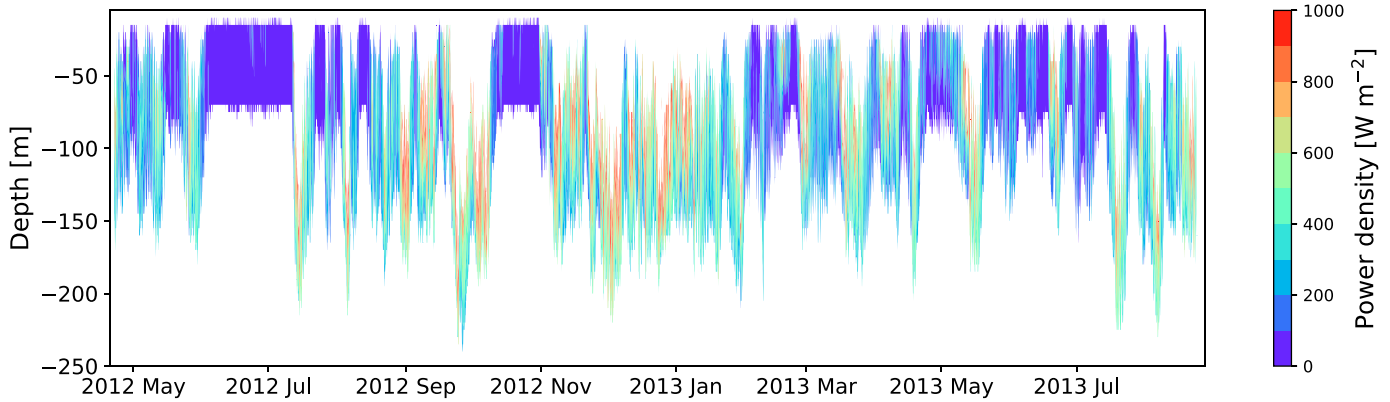

Fig. 6. Temporal evolution over depth of power density computed at EAC2 mooring (location shown in Fig. 1). Note the varying depth of the measurements due to the vertical displacement of the mooring line during episodes of strong current velocity.

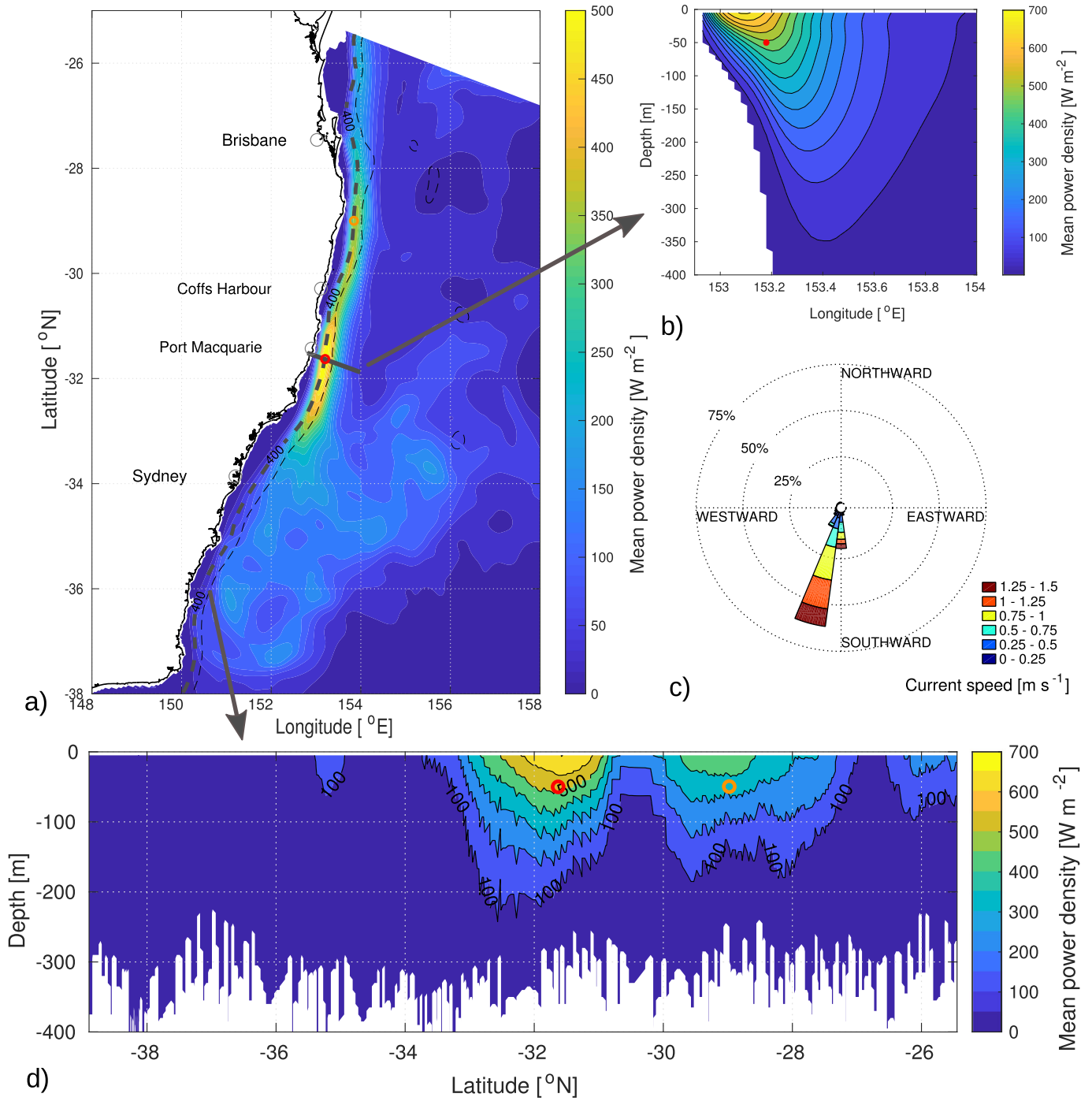

Fig. 7. Modelling results: Mean power density sections in (a) longitude-latitude at 50 m depth, (b) in longitude-depth along the Port Macquarie section normal to the coast at 31.5° S, and (d) in latitude-depth along the 400 m isobath shown in (a) by thick dashed line. The best site is along the Port Macquarie section, above the 400 m isobath and at 50 m depth, and is indicated by the red circles in panels (a, b, d). The second best site is at 29°S, denoted by orange circles in (a, d). In panel (c), a rose plot of current velocity shows the range of directions and intensities at the best site. The dashed contours in panel (a) show the 400 m and 2000 m isobaths and main coastal cities (grey open circles). The section in panel (b) is used to estimate the EAC power in Fig. 8. (For interpretation of the references to color in this figure legend, the reader is referred to the web version of this article.)

shown by the cross-isobath transect off Port Macquarie (~ 31.5°, location shown in Fig. 7a) where the EAC encroaches the continental slope due to the narrow shelf (Fig. 7b), accelerates to become the fastest mean flow along the east Australian coast, and thus provides the best prospective site for power extraction. At this latitude, the 100 W m^{-2} contour extends down to 350 m, with the core of the EAC only a few kilometers from the coastline. At 50 m depth, the average P_d is 489 W m^{-2} and the current speed is greater than the cut-in speed (0.5 m s^{-1}) 76% of the time (Table 1). In terms of current direction - another important variable to consider - the site exhibits a consistent southward flow (median direction of 12°) 74% of the time (Fig. 7c and Table 1).

The second best site along the east coast appears to be at 29.1°S, with a mean P_d of 333 W m^{-2} at 50 m above the 400 m isobath, and consistent flow above the cut-in speed 70% of the time (Table 1).

Table 1
Statistics at two sections at 50 m depth above the 400 m isobath (see location in Fig. 7, red and orange symbols): modelled mean power density and percentage of time the speed S > 0.5 m s^{-1}, median current direction from which it originates (degrees clockwise from the north) and percentage of time the direction is within 10° of the median. Section at ~ 31.5°S is the Port Macquarie section shown in Fig. 7.

Section latitude	Mean P_d [W m^{-2}]	Time S > 0.5 m s^{-1} [%]	Median direction [°]	Time direction ± 10° [%]
~ 29°S	332	70	6	67
~ 31.5°S	489	76	12	74

7. Discussion

This is the first observational high-resolution study assessing the EAC as a renewable energy resource. We have shown that the Australian WBC has the potential to provide energy for the nearby populated coastline, although its power is weaker compared to other WBCs. Archer et al. (2018) highlighted a similar cross-shelf structure between the Florida current and the EAC, but also a larger meandering signal in the EAC. This is reflected in the difference between the power density of the EAC core and at a fixed point (Fig. 2), and explains why the mean EAC hydrokinetic flow is relatively weak. However, large arrays of turbines covering a few tens of kilometers would allow the extraction of a maximum power despite the meandering of the flow. While other locations (Gulf Stream, Aghulas Currents, Kuroshio, Dhanak et al., 2016; VanZwieten et al., 2013; Tseng et al., 2017) seem more adequate for large scale programs, the EAC should be kept in mind for regional studies, especially as technological feasibility and rentability improve. Besides, turbines are likely to have a maximum rotation rate, meaning that no extra power can be extracted for velocities greater than a threshold (e.g. 1.7 m s^{-1}, Bane et al., 2017). This limitation could be an advantage for the EAC, where the current speed rarely exceeds 2 m s^{-1} (Fig. 7c) which reduces the effort on the mechanical structures.

Quantitatively, a cut-in flow speed of 0.5 m s^{-1} which has recently been considered necessary for the device to start producing power (Bane et al., 2017; Meyer et al., 2017), makes energy extraction possible in the EAC most of the time. However, the annual variability should be taken into account, and the site should be chosen carefully due to the great meridional variability in the EAC speed and topographic differences in the region. Data from an assimilating model resolving the continental shelf highlight an optimal location around 31.5°S, 25 km off the city of Port Macquarie, where the power could be extracted 74% of the time at 50 m depth with a relatively easy anchorage (water depth of 400 m). Since only around 2% of the areas where P_d > 500 W m^{-2} are within 25 km of land globally (VanZwieten et al., 2013), the average density of 489 W m^{-2} at that site makes it a promising location for energy extraction.

In order to estimate the MKE power, the power density needs to be multiplied by the swept area of the ocean turbine A. Hypothetical blade diameters of d = 33 m (Bane et al., 2017) lead to $A = \pi d^2/4 \sim 855$ m^2. However, only a portion of this power can actually be extracted, with a theoretical maximum fraction of 59% (the Betz limit, e.g. Hanson et al., 2016). In reality, the final fraction of delivered electrical power is estimated around 40% due to a fraction remaining in the flow or converted to heat during transmission (Bane et al., 2017; Li et al., 2017).

Assuming an average power density of 489 W m^{-2} at our selected site with an overall efficiency of 40% (similar to Yang et al. (2015)), the

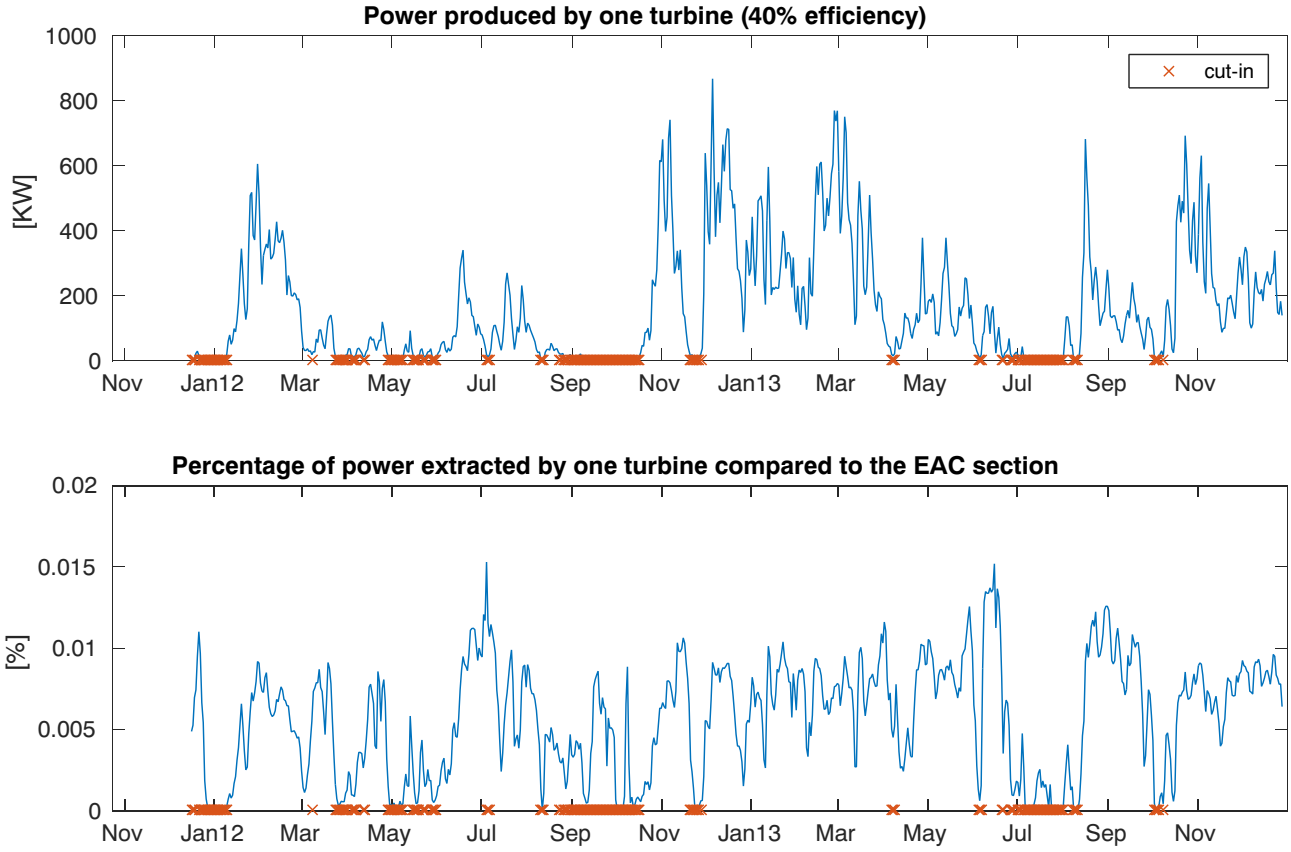

Fig. 8. Modelling results at Port Macquarie site (shown in Fig. 7b). (a) Time-series of power hypothetically produced by one turbine with 40% efficiency and cut-in times (S < 0.5 m s^{-1}). (b) Percentage of power hypothetically extracted by one turbine compared to the undisturbed power of the EAC (see EAC box in Fig. 7b). See text for details (Section 7).

mean extractable power per device would be of the order of $P = 0.4 * 489 * 855 \simeq 167$ kW. The time-series however show high variability (Fig. 8a), with periods reaching weeks of non-extractable power due to the cut-in speed, and peaks reaching 850 KW. This is certainly weak compared to the Florida or Agulhas currents where current speeds are higher, but has potential to be significantly increased when considering many and larger turbines or greater seawater depths.

Compared to the undisturbed kinetic flow of the EAC (e.g. through the EAC box shown in Fig. 7b), one turbine would extract less than 0.015% of the EAC power. Consequently, an array of 60 turbines would still only reduce the EAC energy by less the 1%, which is unlikely to significantly affect the large-scale circulation. This is a consequence of the wide and spread EAC, whose energy is not only concentrated in a narrow jet where turbines would extract it, as opposed to assumptions on the extraction on the Gulf Stream MKE (Yang et al., 2013). That said, turbulence and drag effects could still significantly impact the local fluid dynamics.

Additional environmental considerations are numerous and out of the scope of this study. These considerations include the geomorphology of the seabed (Meyer et al., 2017) and sediment transport, the impact on marine ecosystems (devices are likely to act as fish aggregation, and could impact marine species lethally or behaviourally, Meyer et al., 2017). Moreover, regulatory and social filters will also need to be considered when moving from the research to the pilot phase (Council, 2013). We refer to Hanson et al. (2010) or Dhanak et al. (2016) for more details.

This is an initial estimate of how much renewable energy could be extracted from the EAC, based on observations and a high resolution data-assimilating model, but many uncertainties should be kept in mind. Different designs of devices will affect the hypothetical parameters used in our estimates; in particular, the size and depth of the turbine, and the optimal turbine cluster. Ultimately, pin-pointed in situ current measurements should complement the model-informed 'best-site' estimate made here before any further development plan, and additional considerations could include an economic metric like in Dhanak et al. (2016) and Tseng et al. (2017), with locally determined weights for the size of the area, mean and maximum power density, distance from shore and depth of sea floor.

Acknowledgments

Data was sourced from the Integrated Marine Observing System (IMOS) - an initiative of the Australian Government being conducted as part of the National Collaborative Research Infrastructure Strategy and the Super Science Initiative. We thank two reviewers and the editors for their useful comments on the manuscript. The model development was partially supported by the Australian Research Council grant DP140102337 and LP to MR.

References

Archer, M., Keating, S.R., Roughan, M., Johns, W.E., Lumpkin, R., Beron-Vera, F.J., Shay, L.K., 2018. The kinematic similarity of two western boundary currents revealed by sustained high-resolution observations. Geophys. Res. Lett. 45, 6176–6185. https://doi.org/10.1029/2018GL078429.

Archer, M.R., Roughan, M., Keating, S.R., Schaeffer, A., 2017. On the variability of the East Australian Current: jet structure, meandering, and influence on shelf circulation. J. Geophys. Res. Oceans 122, 8464–8481. https://doi.org/10.1002/2017JC013097.

Archer, M.R., Shay, L.K., Johns, W.E., 2017. The surface velocity structure of the Florida Current in a jet coordinate frame. J. Geophys. Res. Oceans 122, 9189–9208. https://doi.org/10.1002/2017JC013286.

Archer, M.R., Shay, L.K., Martinez-Pedraja, J., 2015. Evaluation of wera hf radar observations: currents, winds and waves. In: 2015 IEEE/OES Eleveth Current, Waves and Turbulence Measurement (CWTM), pp. 1–9. https://doi.org/10.1109/CWTM.2015.7098148.

Bane, J., He, R., Muglia, M., Lowcher, C., Gong, Y., Haines, S., 2017. Marine hydrokinetic energy from western boundary currents. Annu. Rev. Mar. Sci. 9 (1), 105–123. https://doi.org/10.1146/annurev-marine-010816-060423.

Cetina-Heredia, P., Roughan, M., van Sebille, E., Coleman, M.A., 2014. Long-term trends in the East Australian Current separation latitude and eddy driven transport. J. Geophys. Res. Oceans 119, 4351–4366. https://doi.org/10.1002/2014JC010071.

Chapman, R.D., Shay, L.K., Graber, H.C., Edson, J.B., Karachintsev, A., Trump, C.L., Ross, D.B., 1997. On the accuracy of hf radar surface current measurements: intercomparisons with ship-based sensors. J. Geophys. Res. Oceans 102, 18737–18748. https://doi.org/10.1029/97JC00049.

Chang, Y.-C., Chu, P.C., Tseng, R.-S., 2015. Site selection of ocean current power generation from drifter measurements. Renew. Energy 80, 737–745. https://doi.org/10.1016/j.renene.2015.03.003.

Chen, F., 2010. Kuroshio power plant development plan. Renew. Sust. Energ. Rev. 14, 2655–2668. https://doi.org/10.1016/j.rser.2010.07.070.

Chen, H., Tang, T., Ait-Ahmed, N., Benbouzid, M.E.H., Machmoum, M., Zaim, M.E., 2018. Attraction, challenge and current status of marine current energy. IEEE Access 6, 12665–12685. https://doi.org/10.1109/ACCESS.2018.2795708.

Cosoli, S., Grcic, B., De Vos, S., Hetzel, Y., 2018. Improving data quality for the Australian high frequency ocean radar network through real-time and delayed-mode quality-control procedures. Remote Sens. 10. https://doi.org/10.3390/rs10091476.

Council, N.R., 2013. An Evaluation of the U.S. Department of Energy's Marine and Hydrokinetic Resource Assessments. The National Academies Press, Washington, DC. https://doi.org/10.17226/18278. https://www.nap.edu/catalog/18278/an-evaluation-of-the-us-department-of-energys-marine-and-hydrokinetic-resource-assessments.

Deng, X., Griffin, D., Ridgway, K., Featherstone, J., White, N., Cahill, M., 2010. Satellite altimetry for geodetic, oceanographic and climate studies in the Australian region. Coastal Altimetry, Springer, Berlin. https://doi.org/10.1007/978-3-642-12796-0_18.

Dhanak, M.R., Duerr, A.E., VanZwieten, J.H., 2016. Marine Hydrokinetic Energy Resource Assessment. Springer International Publishing, Cham, pp. 1099–1116. https://doi.org/10.1007/978-3-319-16649-0_44.

Esteban, M., Leary, D., 2012. Current developments and future prospects of offshore wind and ocean energy. Appl. Energy 90, 128–136.

Griffin, D., Hemer, M., 2010. Ocean power for Australia - waves, tides and ocean currents. In: OCEANS'10 IEEE SYDNEY, pp. 1–3. https://doi.org/10.1109/OCEANSSYD.2010.5603609.

Gurgel, K., Essen, H.-H., Kingsley, S., 1999. High-frequency radars: physical limitations and recent developments. Coast. Eng. 37, 201–218. https://doi.org/10.1016/S0378-3839(99)00026-5.

Hammar, L., Ehnberg, J., Mavume, A., Cuamba, B.C., Molander, S., 2012. Renewable ocean energy in the western Indian Ocean. Renew. Sust. Energ. Rev. 16, 4938–4950. https://doi.org/10.1016/j.rser.2012.04.026.

Hanson, H.P., Skemp, S.H., Alsenas, G.M., Coley, C.E., 2010. Power from the Florida Current: a new perspective on an old vision. Bull. Am. Meteorol. Soc. 91, 861–867. https://doi.org/10.1175/2010BAMS3021.1.

Hanson, H.P., VanZwieten, J.H., Alsenas, G.M., 2016. Ocean Current Energy Conversion. Springer International Publishing, Cham, pp. 1147–1162. https://doi.org/10.1007/978-3-319-16649-0_46.

Imawaki, S., Bower, A.S., Beal, L., Qiu, B., 2013. Chapter 13 - western boundary currents. In: Gerold Siedler, J.G., Griffies, Stephen M., Church, J.A. (Eds.), Ocean Circulation and ClimateA 21st Century Perspective. International Geophysics, vol. 103. Academic Press, pp. 305–338. https://doi.org/10.1016/B978-0-12-391851-2.00013-1.

Kerry, C., Powell, B., Roughan, M., Oke, P., 2016. Development and evaluation of a high-resolution reanalysis of the East Australian Current region using the Regional Ocean Modelling System (ROMS 3.4) and Incremental Strong-Constraint 4-Dimensional Variational (IS4D-Var) data assimilation. Geosci. Model Dev. 9, 3779–3801. https://doi.org/10.5194/gmd-9-3779-2016.

Kerry, C., Roughan, M., Powell, B., 2018. Observation impact in a regional reanalysis of the East Australian Current System. J. Geophys. Res. Oceans 123, 7511–7528. https://doi.org/10.1029/2017JC013685.

Li, B., de Queiroz, A.R., DeCarolis, J.F., Bane, J., He, R., Keeler, A.G., Neary, V.S., 2017. The economics of electricity generation from gulf stream currents. Energy 134, 649–658. https://doi.org/10.1016/j.energy.2017.06.048.

Lowcher, C.F., Muglia, M., Bane, J.M., He, R., Gong, Y., Haines, S.M., 2017. Marine Hydrokinetic Energy in the Gulf Stream Off North Carolina: An Assessment Using Observations and Ocean Circulation Models. Springer International Publishing, Cham, pp. 237–258. https://doi.org/10.1007/978-3-319-53536-4_10.

Mata, M., Wijffels, S., Church, J., Tomczak, M., 2006. Statistical description of the East Australian Current low-frequency variability from the WOCE PCM3 array. Mar. Freshwater Res. 57, 273–290.

Meyer, I., Braby, L., Krug, M., Backeberg, B., 2017. Mapping the Ocean Current Strength and Persistence in the Agulhas to Inform Marine Energy Development. Springer International Publishing, Cham, pp. 179–215. https://doi.org/10.1007/978-3-319-53536-4_8.

Moore, A.M., Arango, H.G., Broquet, G., Powell, B.S., Weaver, A.T., Zavala-Garay, J., 2011. The regional ocean modeling system (roms) 4-dimensional variational data assimilation systems: part i – system overview and formulation. Prog. Oceanogr. 91, 34–49. https://doi.org/10.1016/j.pocean.2011.05.004.

Neary, V., Lawson, M., Previsic, M., Copping, A., Hallett, K., LaBonte, A., Rieks, J., Murray, D., 2014. Methodology for design and economic analysis of marine energy conver sion (MEC) technologies. In: Proceedings of the 2nd Marine Energy Technology Symposium METS14 April 15-18, 2014, Seattle, WA..

O'Callaghan, B., Chabchouc, A., 2018. Advances in Renewable Energies Offshore: Proceedings of the 3rd International Conference on Renewable Energies Offshore (RENEW 2018), October 8–10, 2018, Lisbon, Portugal. CRC Press, pp. 31–38.

Oke, P.R., Pilo, G.S., Ridgway, K., Kiss, A., Rykova, T., 2019. A search for the tasman front. J. Mar. Syst. 199, 103217. https://doi.org/10.1016/j.jmarsys.2019.103217.

Schaeffer, A., Roughan, M., 2015. Influence of a western boundary current on shelf dynamics and upwelling from repeat glider deployments. Geophys. Res. Lett. 42, 121–128. https://doi.org/10.1002/2014GL062260.

Schaeffer, A., Roughan, M., Austin, T., Everett, J.D., Griffin, D., Hollings, B., King, E., Mantovanelli, A., Milburn, S., Pasquer, B., Pattiaratchi, C., Robertson, R., Stanley, D., Suthers, I., White, D., 2016. Mean hydrography on the continental shelf from 26 repeat glider deployments along Southeastern Australia. Sci. Data 3, 160070. https://doi.org/10.1038/sdata.2016.70.

Schaeffer, A., Roughan, M., Morris, B., 2013. Cross-shelf dynamics in a Western Boundary Current. Implications for upwelling. J. Phys. Oceanogr. 43, 1042–1059. https://doi.org/10.1175/JPO-D-12-0177.1.

Schaeffer, A., Roughan, M., White, D., Jones, E., 2016. Physical and biogeochemical spatial scales of variability in the East Australian Current separation zone from shelf glider measurements. Biogeosciences 13. https://doi.org/10.5194/bg-13-1967-2016.

Sloyan, B.M., Ridgway, K.R., Cowley, R., 2016. The East Australian Current and property transport at 27°S from 2012 to 2013. J. Phys. Oceanogr. 46, 993–1008. https://doi.org/10.1175/JPO-D-15-0052.1.

Tseng, R.-S., Chang, Y.-C., Chu, P.C., 2017. Use of Global Satellite Altimeter and Drifter Data for Ocean Current Resource Characterization. Springer International Publishing, Cham, pp. 159–177. https://doi.org/10.1007/978-3-319-53536-4_7.

VanZwieten, J.H., Meyer, I., Alsenas, G.M., 2014. Evaluation of hycom as a tool for ocean current energy assessment. In: Proceedings of the 2nd Marine Energy Technology Symposium METS14 April 15-18, 2014, Seattle, WA..

VanZwieten, J.H., Smentek, A.E., Alsenas, G.M., Hanson, H.P., 2013. Global ocean current energy assessment: an initial look. In: Proceedings of the 1st Marine Energy Technology Symposium METS13 April 10–11, 2013, Washington, DC..

Wood, J., Schaeffer, A., Roughan, M., Tate, P., 2016. Seasonal variability in the continental shelf waters off southeastern Australia: fact or fiction? Cont. Shelf Res. 112, 92–103. https://doi.org/10.1016/j.csr.2015.11.006.

Wyatt, L.R., Mantovanelli, A., Heron, M.L., Roughan, M., Steinberg, C.R., 2018. Assessment of surface currents measured with high-frequency phased-array radars in two regions of complex circulation. IEEE J. Ocean. Eng. 43, 484–505. https://doi.org/10.1109/JOE.2017.2704165.

Yang, X., Haas, K.A., Fritz, H.M., 2013. Theoretical assessment of ocean current energy potential for the Gulf Stream system. Mar. Technol. Soc. J. 47, 101–112. https://doi.org/10.4031/MTSJ.47.4.3.

Yang, X., Haas, K.A., Fritz, H.M., French, S.P., Shi, X., Neary, V.S., Gunawan, B., 2015. National geodatabase of ocean current power resource in USA. Renew. Sust. Energ. Rev. 44, 496–507. https://doi.org/10.1016/j.rser.2015.01.007.